

Scale Effects on Cavitation about a Sphere

J. A. Venning¹, B. W. Pearce¹ and P. A. Brandner¹

¹ University of Tasmania, Launceston, Tasmania, 7250, Australia

Abstract

The cavity topology about a sphere is provided for a range of Reynolds numbers from 1.25×10^5 to 1.5×10^6 . This decade range was achieved through three different diameter spheres and changing the freestream velocity. Various cavitation regimes were investigated including sheet cavitation, unsteady shedding of cloud cavitation, and supercavitation. High-resolution photography was used to capture the cavity state and allowed measurement of the cavity detachment angle. Two Reynolds number transitions were observed. Comparisons of cavity appearance at the same Reynolds and cavitation numbers, but different physical scales, show the influence of the Weber number.

Keywords

Cavitation; multi-phase flow;

Introduction

The link between the state of a boundary layer and the appearance of attached cavitation on a body was established by [6], who found the cavity attachment is dependent on a laminar separation in the boundary layer upstream of the cavity. The distance between the laminar separation bubble and the cavity is dependent on the Reynolds number [2]. For a single-phase flow, the wake and drag of bluff bodies changes at a critical Reynolds number, known as the drag crisis. This was noted by Eiffel [11] who observed the drag of spheres to decrease drastically at a diameter-dependent critical velocity. This has since been attributed to a transition in the boundary layer from laminar to turbulent. After boundary layer transition (supercritical), the turbulent flow remains attached further around the sphere, reducing the width of the wake and thus reducing the drag. The flow state is complicated further by the presence of a laminar

separation bubble which intermittently exists near the Reynolds number transition [9] and is ever-present for $Re > 375 \times 10^3$.

For a supercritical sphere, the cavitation behaviour has been described in [4, 8, 19]. The salient features are a small sheet cavity near inception, the growth and shedding of cloud cavities at moderate cavitation numbers, and the onset of supercavitation near a cavitation number of 0.35.

One of the features of attached cavitation is the appearance of inter-facial cells at the leading edge of the cavity. These cells have been observed in hydraulic bearing crevices [10], weirs, contractions [7], as well as both bluff [17] and streamlined bodies [12, 13, 14]. The surface energy is a critical factor in whether these cells form, with [17] noting that hydrophobic surfaces create the same ‘divots’ as we encounter here. They found that the spanwise breakup of the cells only occurred for low Re , less than 120×10^3 , and the spanwise size of these reduced with Re . The Taylor-Saffman number has been suggested as a controlling factor [15, 16]. [17] also noted that mixing of the water in their blow-down tunnel altered the frequency of the cells. While they attribute this to an increase in the nuclei population, this could also be related to the free-stream turbulence level.

Here we present photographs of the cavitation about a sphere for Reynolds numbers ranging over a decade. The use of several different physical scales allows for the differentiation of viscosity effects from surface tension.

Experimental setup

Experiments were carried out in the Cavitation Research Laboratory water tunnel at the University of Tasmania (figure 1). The tunnel is a variable-pressure facility with absolute pressure

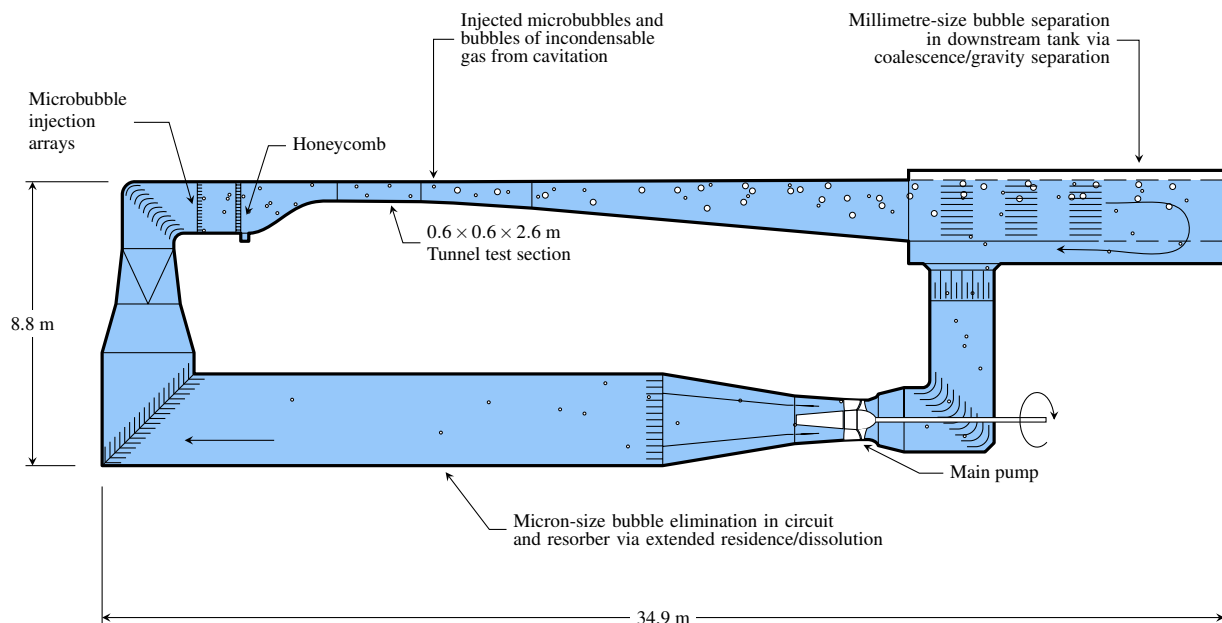


Figure 1. Schematic of the cavitation tunnel showing circuit architecture.

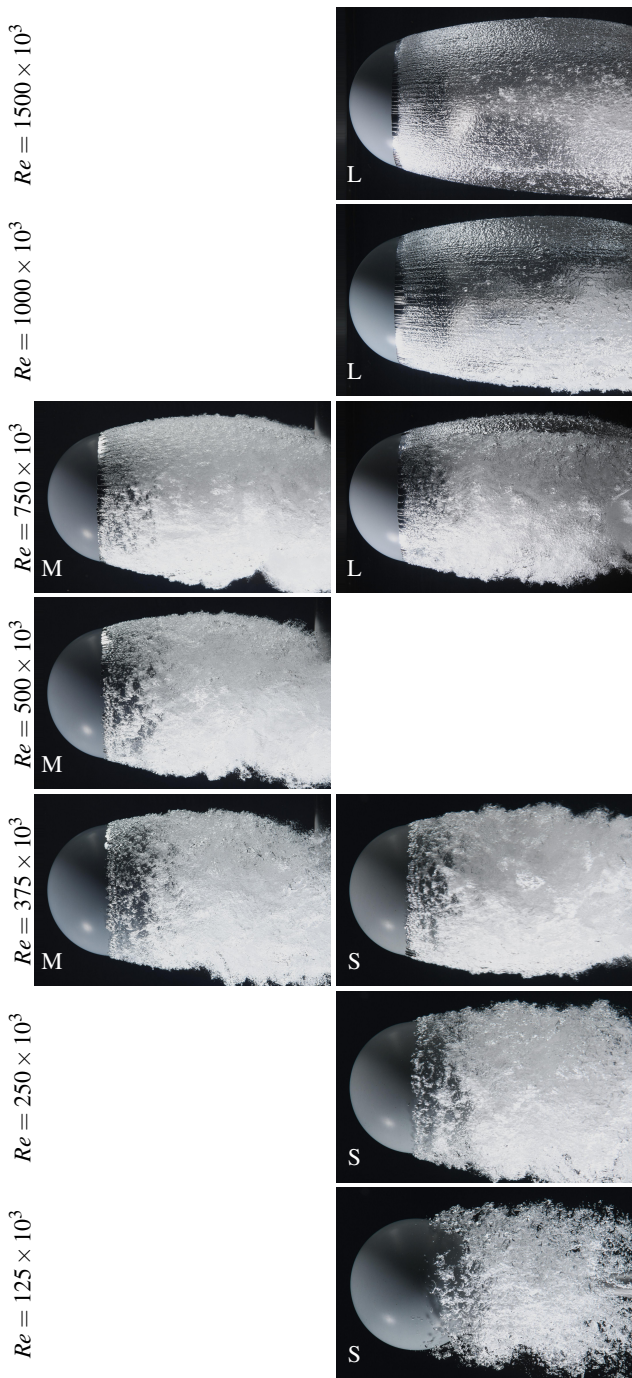


Figure 2. Photographs of the cavity appearance at various Reynolds numbers for a cavitation number of 0.3. The physical scale of the sphere is indicated by an 'S', 'M', or 'L' for the small, medium, and large spheres, respectively. The magnification is altered between the sphere sizes.

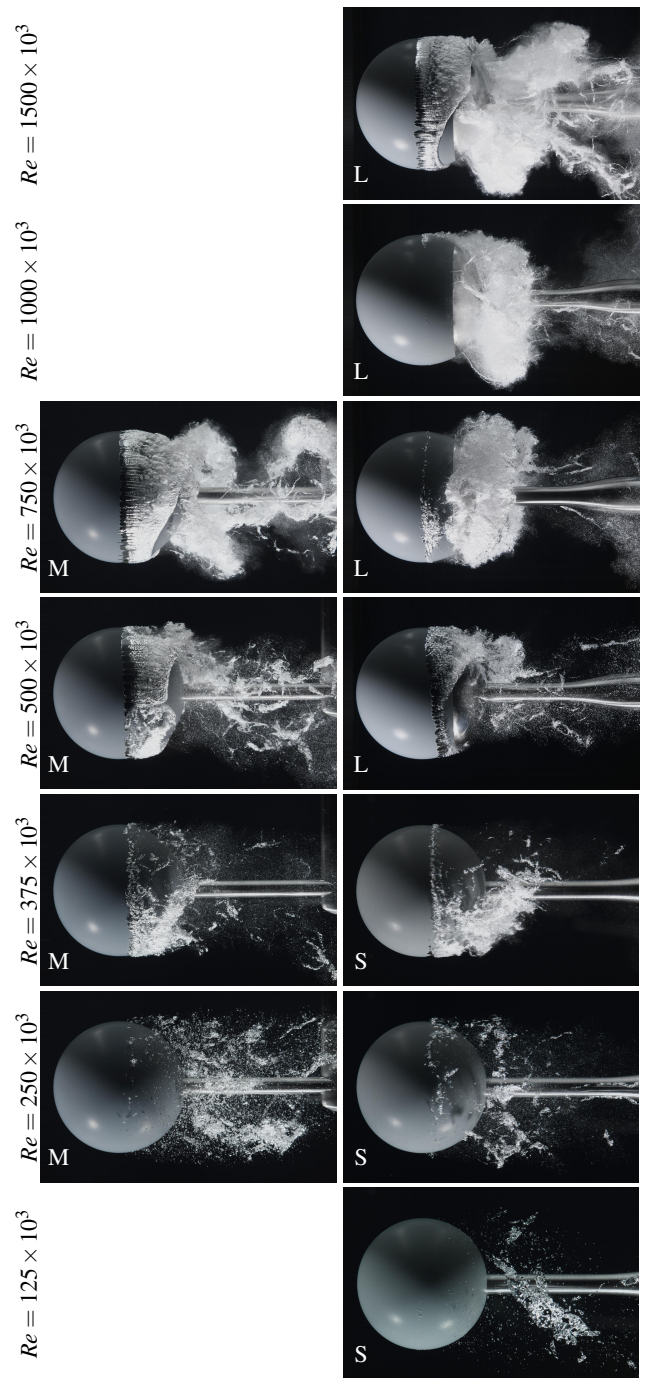


Figure 3. Photographs of the cavity appearance at various Reynolds numbers for a cavitation number of 0.7. The physical scale of the sphere is indicated by an 'S', 'M', or 'L' for the small, medium, and large spheres, respectively. The magnification is altered between the sphere sizes.

range of 4 kPa to 400 kPa. Ancillary systems allow for the strict control of both dissolved oxygen levels and free gas bubbles (additional description is in [3]). For this experiment, no additional nuclei were introduced, such that only the natural nuclei population was active. This population is detailed in [18].

Three spheres were manufactured in order to alter the physical scale in the experiment. The spheres had diameters of 150 mm, 75 mm and 37.5 mm and are labeled the ‘Large’, ‘Medium’ and ‘Small’ spheres, respectively. These spheres were each stung-mounted in the centre of the test section. The front end of each sphere was manufactured out of polyvinyl chloride (PVC).

The Reynolds number,

$$Re = \frac{DU_\infty}{\nu}, \quad (1)$$

where D is the sphere diameter, U_∞ is the freestream velocity, and ν is the kinematic viscosity, was varied from 125×10^3 to 1500×10^3 .

The cavitation number is

$$\sigma = \frac{p_\infty - p_v}{q}, \quad (2)$$

where p_∞ and p_v are the freestream and vapour pressures, respectively, and q is the freestream dynamic pressure. This was set between 0.9 and 0.1 for the experiment, though this paper focuses on supercavitation ($\sigma = 0.3$) and cloud cavitation ($\sigma = 0.7$).

The Weber number relates the fluid inertia to the surface tension, and is:

$$We = \frac{\rho U_\infty^2 D}{s}, \quad (3)$$

where ρ is the water density and s is the surface tension. The water temperature was monitored and the freestream pressure and velocity altered to maintain the desired Reynolds and cavitation numbers.

Photographs of the cavitation appearance at each condition were acquired with a Nikon D850 digital camera. The camera was

used with various lenses according to the sphere size, 60 mm for the large sphere, 105 mm for the medium, and a variable focal length lens set to 150 mm for the small sphere. These lenses, in conjunction with the working distance, allowed the same relative magnification for each photograph. Light was provided by stroboscopic flash lamps by Drello. While the blockage inevitably changes between the cases, the blockage ratio for the most severe case was less than 5%.

Results

Photographs are given in figures 2 and 3 for the supercavitating ($\sigma = 0.3$) and the cloud cavitation ($\sigma = 0.7$), respectively. The size of the sphere is indicated by the ‘L’, ‘M’ or ‘S’ for the large, medium and small spheres, respectively. It was possible to achieve the same Reynolds number between the sizes for several cases through a velocity ratio of 2. This allows a comparison between Weber numbers while maintaining constant Reynolds and cavitation numbers.

Below a Reynolds number of 200×10^3 , the cavitation appears further downstream than above this transition. This is particularly evident for $\sigma = 0.7$, where above $Re = 200 \times 10^3$, the cavity appearance angle only gradually increases as the Re is reduced. The cavity appears here as very large vapour volumes, which may be related to the low Weber numbers for these cases. For $\sigma = 0.7$, cavitation appears only in the wake. A second transition is observed where the leading-edge cells appear. This critical Re is a function of the cavitation number, and is between 375×10^3 and 438×10^3 for $\sigma = 0.3$ and between 438×10^3 and 500×10^3 for $\sigma = 0.7$. The size of the cloud cavities increase with Reynolds number. The supercavity becomes more coherent at high Re , and the surface of the cavity appears to be smoother.

Figure 4 has the angle of the first appearance of cavitation, as measured from the stagnation point, for the range of Reynolds numbers. The higher the cavitation number, the further downstream the cavitation appears, as less tension is applied. The angle moves rearwards as the Reynolds number is reduced. For comparison, the single-phase measurements of the boundary layer separation angle from [1] are given with the black dots.

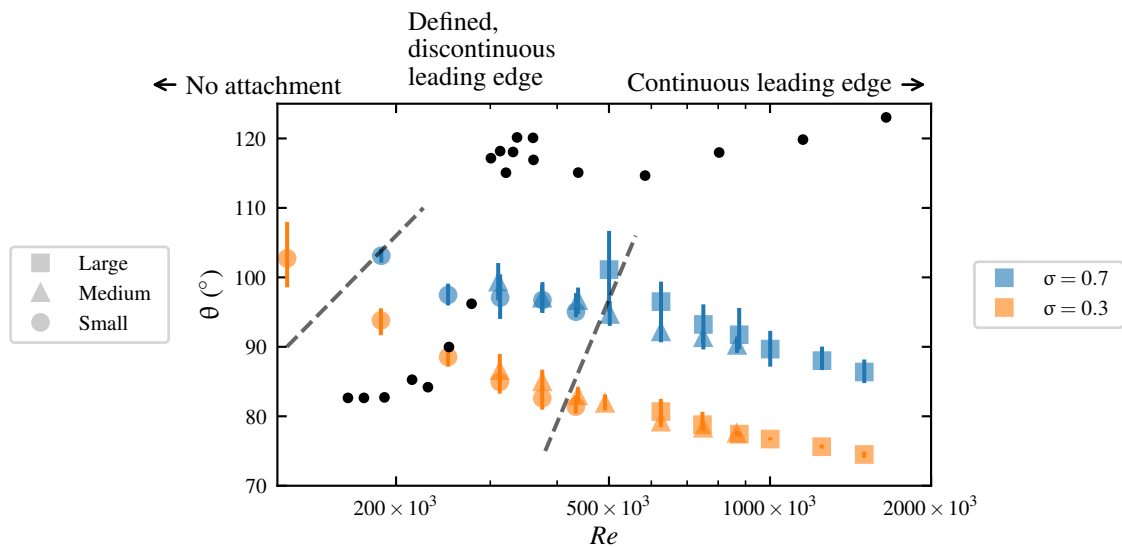


Figure 4. Cavitation appearance angle (measured from stagnation point) for each combination of Reynolds and cavitation numbers. The vertical bars indicate the range of the measurements. The dashed line indicate the two transition between detached (left), a defined though discontinuous leading edge (centre), and attached (right) cavitation. The black dots represent the boundary layer separation angle from [1].

For all the attached cavitation cases, the cavity angle is well upstream of the single-phase result. If the boundary layer does not transition (low Re), the first appearance of cavitation is not attached and appears downstream of the single-phase detachment angle. This all supports the findings of [6] that a laminar separation is necessary for the attached cavitation to occur.

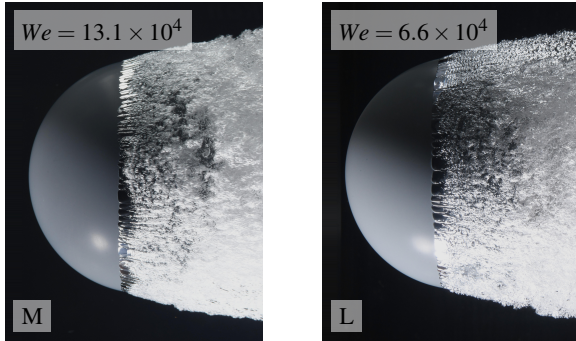


Figure 5. Comparison of the leading-edge cell structure at a common Reynolds number but different Weber numbers. The medium sphere (left) has twice the velocity than the large sphere (right), which has larger cells.

Figure 5 has photographs of the leading-edge interfacial cell structure at common Reynolds and cavitation numbers, but different physical scales. It is interesting to note that the cells appear less regularly than in previous studies in the same laboratory (eg. [4]), but prior to replacement of the water. A similar observation was noted by [17] who noted the regularity of the cells to be improved with the addition of long-chain polymers in [5]. It is conceivable that some biological elements in the water caused the previously observed regularity in the cells. At low Reynolds number, these cells are very stable, lasting some minutes, and in these stable cells condensation droplets are even observable. At fixed Reynolds and cavitation numbers, the size of the cells, relative to the diameter, is always less at the higher velocity (higher Weber number). This suggests that the size of these cells is dependent on the Weber number.

Conclusions

Photographs are presented of cavitation about a sphere for Reynolds numbers spanning a decade. The angle of the first appearance of cavitation is a function of both the Reynolds and cavitation numbers. Two transitions are observed, one related to the appearance of cavitation near the body, and one with the attachment of the cavity onto the surface. The interfacial cells associated with the attached cavitation were shown to be dependent on the Weber number, not solely the Reynolds number.

Acknowledgements

The authors thank Dong Han for his assistance with the acquisition of the photographs. The authors acknowledge the support of the Defence Science and Technology Group.

References

[1] Achenbach, E., Experiments on the flow past spheres at very high Reynolds numbers, *Journal of Fluid Mechanics*, **54**, 1972, 565–575.
 [2] Arakeri, V. H., Viscous effects on the position of cavitation separation from smooth bodies, *Journal of Fluid Mechanics*, **68**, 1975, 779–799.

[3] Brandner, P. A., Lecoffre, Y. and Walker, G. J., Development of an Australian National Facility for Cavitation Research, in *Sixth International Symposium on Cavitation*, 2006, number September, 1–9, 1–9.
 [4] Brandner, P. A., Walker, G. J., Niekamp, P. N. and Anderson, B., An experimental investigation of cloud cavitation about a sphere, *Journal of Fluid Mechanics*, **656**, 2010, 147–176.
 [5] Brennen, C., Some cavitation experiments with dilute polymer solutions, *Journal of Fluid Mechanics*, **44**, 1970, 51–63.
 [6] Briançon-Marjollet, L., Franc, J.-P. and Michel, J.-M., Transient bubbles interacting with an attached cavity and the boundary layer, *Journal of Fluid Mechanics*, **218**, 1990, 355–376.
 [7] Croci, K., Ravelet, F., Danlos, A., Robinet, J.-C. and Barast, L., Attached cavitation in laminar separations within a transition to unsteadiness, *Physics of Fluids*, **31**, 2019, 063605.
 [8] de Graaf, K., Brandner, P. and Pearce, B., Spectral content of cloud cavitation about a sphere, *Journal of Fluid Mechanics*, **812**.
 [9] Deshpande, R., Kanti, V., Desai, A. and Mittal, S., Intermittency of laminar separation bubble on a sphere during drag crisis, *Journal of Fluid Mechanics*, **812**, 2017, 815–840.
 [10] Dowson, D. and Taylor, C., Cavitation in bearings, *Annual Review of Fluid Mechanics*, **11**, 1979, 35–65.
 [11] Eiffel, G., Sur la résistance des sphères dans l'air en mouvement, *Comptes Rendus*, **155**, 1912, 1597–1599.
 [12] Giosio, D., Pearce, B. and Brandner, P., Leading edge interfacial phenomena of sheet and cloud cavitation, in *20th Australasian Fluid Mechanics Conference (20AFMC)*, 2016, 1–4, 1–4.
 [13] Russell, P. S., Giosio, D. R., Venning, J. A., Pearce, B. W. and Brandner, P. A., Microbubble generation from condensation and turbulent breakup of sheet cavitation, in *31st Symposium on Naval Hydrodynamics*, Monterey, 2016.
 [14] Russell, P. S., Venning, J. A., Brandner, P. A., Pearce, B. W., Giosio, D. R. and Ceccio, S. L., Microbubble disperse flow about a lifting surface, in *32nd Symposium on Naval Hydrodynamics*, 2018.
 [15] Savage, M., Cavitation in lubrication. part 1. on boundary conditions and cavity—fluid interfaces, *Journal of Fluid Mechanics*, **80**, 1977, 743–755.
 [16] Savage, M., Cavitation in lubrication. part 2. analysis of wavy interfaces, *Journal of Fluid Mechanics*, **80**, 1977, 757–767.
 [17] Tassin Leger, A., Bernal, L. and Ceccio, S., Examination of the flow near the leading edge of attached cavitation. part 2. incipient breakdown of two-dimensional and axisymmetric cavities, *Journal of Fluid Mechanics*, **376**, 1998, 91–113.
 [18] Venning, J., Khoo, M., Pearce, B. and Brandner, P., Background nuclei measurements and implications for cavitation inception in hydrodynamic test facilities, *Experiments in Fluids*, **59**, 2018, 71.
 [19] Venning, J. A., Giosio, D. R., Pearce, B. W. and Brandner, P. A., Global mode visualization in cavitating flows, in *Proceedings of the 10th International Symposium on Cavitation (CAV2018)*, 2018, volume 2, 485–490, 485–490.